Int. J. Solids Structures Vol. 26, No. 11, pp. 1275–1285, 1990
Printed in Great Britain.

0020–7683/90 $3.00 + .00

INERTIAL EFFECTS ON NECKING IN TENSION

P. TUĞCU, K. W. NEALE and A. E. LAHOUD
Faculty of Applied Science, Université de Sherbrooke, Sherbrooke, Québec, Canada J1K 2R1

(*Received* 7 *July* 1989; *in revised form* 7 *November* 1989)

Abstract—A one-dimensional finite element program has been developed to study the effects of inertia on necking instability in a round bar under tension. An elastic–viscoplastic constitutive law is employed to model the material behaviour of solids with strain and strain-rate hardening characteristics. Necking is initiated by prescribing a geometric imperfection in the form of an area defect in the initial undeformed state. The entire load–deformation–time response from this state is computed. Key features of necking under dynamic conditions are contrasted with static behaviour and with certain aspects of recent similar studies on dynamic effects. Mesh sensitivity resulting from the one-dimensionalization of the formulation is also discussed.

1. INTRODUCTION

A characteristic feature of the deformation of a round ductile specimen under uniaxial tension is the process of necking leading to fracture. Detailed studies of the neck initiation and localization phases have long since appeared for quasi-statically deforming rate-independent solids using both the bifurcation-of-equilibrium approach and analyses where imperfections are introduced to trigger the localization of the deformation. Rate-dependent materials, on the other hand, do not exhibit bifurcations in this sense. The necking phenomena, however, remain similar to those observed for rate-independent solids. One way of modelling localization in rate-dependent materials is by considering an initial geometric or material defect in the specimen. Localization can also occur as a result of inhomogeneous states of stress and deformation arising from the particular boundary-value problem.

Numerous works dealing with various aspects of necking can be found in the literature. Most of these studies consider quasi-static loading conditions. Material rate dependence is accounted for in Hutchinson and Neale (1977) and Needleman and Tvergaard (1985), where the stabilizing effect of strain-rate sensitivity is demonstrated.

In contrast, the study of the effects of inertia on neck localization has been rather limited. Taylor *et al.* (1978) studied dynamic instabilities in a rate-sensitive thin sheet using a one-dimensional hydrodynamic flow analogy. The effects of inertia in an axisymmetric specimen were analysed numerically by Regazzoni *et al.* (1986) for a rate and temperature-dependent solid. Needleman (1989) recently studied shear band development including the effects of the inertia for viscoplastic solids. The softening effect due to deformation-induced heating was also included in his analysis. Using the finite element method, he determined the entire load–deformation–time response from the initial unloaded state. In the analyses of Taylor *et al.* (1978) and Regazzoni *et al.* (1986), the specimen is assumed initially to be deforming homogeneously up to a certain state of uniform plastic strain. A perturbation in the form of a geometric imperfection is then introduced at this strain to initiate necking, and the evolution of this perturbation is simulated. In all of the above studies the stabilizing effect of inertia was demonstrated.

In the present analysis, necking in an axisymmetric specimen, including the effects of inertia and strain-rate sensitivity, is studied using a one-dimensional model. In contrast to the approach adopted by Regazzoni *et al.* (1986), we introduce a geometric defect in the *initial* unloaded state and compute the entire load–deformation–time response of the specimen from this state. This approach is analogous to the long-wavelength analysis employed by Hutchinson and Neale (1977) and, as discussed there, such an analysis is believed to be accurate enough to reveal the key features of instability in tension. An elastic–viscoplastic constitutive model is used. An explicit integration method based on the

Newmark family of algorithms is employed for the integration of the governing equations, while a direct Euler integration scheme is used for updating the stresses. The consistent mass matrix approach is adopted for the solution of the governing equations of the one-dimensional finite element grid. Solids with both rate-independent and rate-dependent material response are analysed. The quasi-static solution is first obtained as a limiting case from the dynamic solution by employing an extremely low pull speed. This serves as a check on the separate finite element program developed to obtain the solutions for quasi-static behaviour.

Mesh sensitivity arising from the localization of the deformations in one single element at the neck is a result of the one-dimensionalization of the problem. This aspect is also discussed.

2. PROBLEM FORMULATION

An incompressible solid circular specimen with nominal radius R_0 and length $2L_0$ in the initial undeformed state is considered. A Lagrangian, one-dimensional formulation is adopted where material points are labelled by their convected coordinates x along the axis of the bar in the initial reference configuration. The origin of the x-axis is located at the mid-section of the specimen and symmetry about $x = 0$ is assumed. Due to this symmetry only one half of the bar is analysed numerically.

At time $t = 0$, a pull velocity $\dot{U} = \text{const.}$ is applied to each end of the specimen. The boundary conditions are thus

$$\begin{aligned} \dot{u}(0, t) &= 0 \quad \text{for } t \geqslant 0 \\ \dot{u}(L_0, t) &= \dot{U} \quad \text{for } t \geqslant 0 \end{aligned} \tag{1}$$

where $u(x, t)$ represents the axial displacement and a dot denotes differentiation with respect to time. The axial stretch λ and strain ε are given by

$$\lambda = 1 + \frac{\partial u}{\partial x}, \quad \varepsilon = \ln \lambda. \tag{2}$$

Also because of incompressibility the current cross-sectional area A and initial area A_0 are related through

$$A(x, t) = \frac{A_0(x, 0)}{\lambda}. \tag{3}$$

The load on a given cross-section is $P = \sigma A$ and the equation of motion becomes

$$\frac{\partial}{\partial x}\left(\frac{\sigma}{\lambda}\right) = \rho \ddot{u} \tag{4}$$

where σ is the true (Cauchy) stress and ρ is the density (constant). Multiplying both sides of this equation by $A_0 \delta u$, where δu is an arbitrary virtual displacement field, integrating over the range $0 \rightarrow L$ and using the integration-by-parts formula gives

$$\int_0^{L_0} \left[\rho A_0 \ddot{u} \delta u + \frac{\sigma A_0}{\lambda} \delta u_{,x} \right] \mathrm{d}x = 0. \tag{5}$$

Here a comma denotes partial differentiation. This variational equation forms the basis of the dynamic finite element analysis.

The variational equation for the quasi-static analysis is based on the following differential equation

$$\Delta t\left\{\frac{\partial}{\partial x}\left[\frac{\dot{\sigma}}{\lambda}-\frac{\sigma}{\lambda}\dot{\varepsilon}\right]\right\}+\frac{\partial}{\partial x}\left(\frac{\sigma}{\lambda}\right)=0. \tag{6}$$

In this expression, the second term set equal to zero is the equation of equilibrium [i.e. (4) with $\ddot{u}=0$] and the first is the incremental equilibrium counterpart. Multiplying (6) by $A_0\delta u$ and integrating as described above gives the quasi-static variational relation

$$\Delta t\int_0^{L_0}\left[\frac{\dot{\sigma}A_0}{\lambda}-\frac{\sigma A_0}{\lambda}\dot{\varepsilon}\right]\delta u_{,x}\,\mathrm{d}x+\int_0^{L_0}\frac{\sigma A_0}{\lambda}\delta u_{,x}\,\mathrm{d}x=0. \tag{7}$$

This result is identical to that obtained by expanding the principle of virtual work about the current state (Lahoud *et al.*, 1986).

The strain-rate dependency of the inelastic response of metals at high rates of deformation has been clearly established experimentally. The assumption of rate-independent material behaviour at low strain rates and room temperature remains valid for many applications. Under quasi-static conditions, there is an essential difference between the two descriptions in that localization in the form of bifurcations is possible only for a rate-independent solid. When dynamic effects are included in the analysis, another difference arises between the two formulations: for a rate-independent solid, the propagation speed of a wave is given by the plastic wave speed (i.e. determined by the tangent modulus E_t), in contrast to the rate-dependent solid where waves travel at the elastic wave speed. Since experiments on plastically pre-strained specimens indicate that the incremental disturbances travel at essentially the propagation speed of an elastic wave, inclusion of viscoplastic effects is believed to be more realistic in dynamic problems involving plastic behaviour. A detailed comparison of theory and experiment on this issue, including a vast survey of previous works, has been reported by Clifton (1972).

In our analysis, the rate-dependent solid is modelled using the following elastic viscoplastic constitutive law

$$\frac{\sigma}{\sigma_Y}=\begin{cases}\dfrac{E}{\sigma_Y}\varepsilon & \text{for } \dfrac{\sigma}{\sigma_Y}\leqslant 1\\[2ex] \left(\dfrac{E}{\sigma_Y}\right)^N\left[(\varepsilon^P+\varepsilon_Y)^N+m\ln\left(1+\dfrac{\dot{\varepsilon}^P}{\dot{\varepsilon}_R}\right)\right] & \text{for } \dfrac{\sigma}{\sigma_Y}\geqslant 1\end{cases} \tag{8}$$

In this representation ε^P corresponds to the plastic component of the logarithmic strain ($=\int\dot{\varepsilon}^P\,\mathrm{d}t$), the subscript Y denotes quantities associated with initial yield, m is a strain-rate sensitivity index, $\dot{\varepsilon}_R$ represents a reference strain rate, and N is the strain-hardening exponent. A plot of σ versus ε^P (8) is illustrated in Fig. 1 for $m=0$ (rate-independent material

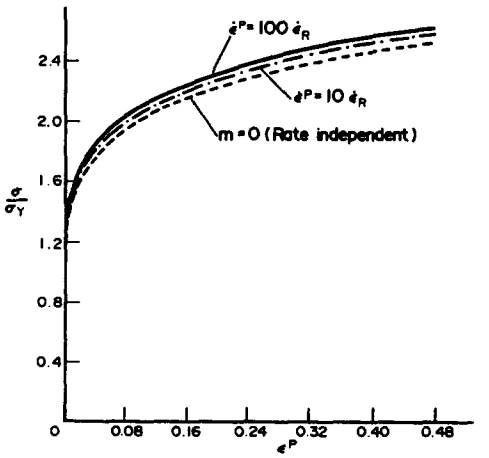

Fig. 1. Uniaxial stress–strain–strain-rate behaviour for varying strain-rate values.

response), and rate-dependent behaviour ($m \neq 0$) with strain rates $\dot{\varepsilon}^P = 10\dot{\varepsilon}_R$ and $100\dot{\varepsilon}_R$. Although this law may not be the most accurate for describing metal behaviour at high strain rates, it should be sufficient for modelling the essential features of the dynamic necking phenomena investigated here. For the rate-independent solid, the form $(\sigma/\sigma_Y) = (E\varepsilon/\sigma_Y)^N$ was employed. In rate form we use the relation

$$\dot{\sigma} = E(\dot{\varepsilon} - \dot{\varepsilon}^P) \tag{9}$$

with $\dot{\varepsilon}^P$ calculated from (8).

To initiate the necking process an initial geometric imperfection of the form $R(x, 0) = R(L_0, 0) + \Delta R$ is introduced, where ΔR is given by

$$\Delta R = -\xi R_0 \exp\left[-\left(\frac{\kappa x}{L_0}\right)^2\right] \tag{10}$$

with $\xi, \kappa > 0$, with an appropriate value of κ to satisfy the long-wavelength assumption.

3. NUMERICAL ANALYSIS

The finite element discretization is implemented using bar elements with linear interpolation functions for the displacement u. The following non-dimensional quantities are introduced:

$$\bar{\sigma} = \frac{\sigma}{\sigma_Y}, \quad a = \frac{A_0(x)}{A_0(L_0)}, \quad \bar{l} = \frac{l}{L_0}, \quad \bar{t} = \frac{c}{L_0}t \tag{11}$$

where l is the length of an element and $c = \sqrt{E/\rho}$ denotes the elastic wave speed. Using the last of (11), we also have

$$\acute{u} = \frac{L_0}{c}\dot{u}, \quad \ddot{u} = \frac{L_0^2}{c^2}\ddot{u} \tag{12}$$

where the prime denotes differentiation with respect to $\bar{t}$.

Substitution of the interpolation functions in the variational principle (5) gives the global equations of motion for the finite element grid

$$\mathbf{M}\ddot{\mathbf{Q}} = \mathbf{R} \tag{13}$$

where the consistent mass matrix $\mathbf{M}$, the nodal acceleration vector $\ddot{\mathbf{Q}}$ and the nodal force vector $\mathbf{R}$ are obtained by assembling the following element mass matrix $\mathbf{m}$, nodal acceleration vector $\ddot{\mathbf{q}}$ and nodal force vector $\mathbf{r}$

$$\mathbf{m} = \frac{E}{\sigma_Y}\frac{a_i\bar{l}_i}{6}\begin{pmatrix} 2 & 1 \\ 1 & 2 \end{pmatrix}$$

$$\ddot{\mathbf{q}} = \begin{pmatrix} \ddot{u}_j \\ \ddot{u}_{j+1} \end{pmatrix}$$

$$\mathbf{r} = \begin{pmatrix} (\bar{\sigma}_i a_i)/\lambda_i \\ -(\bar{\sigma}_i a_i)/\lambda_i \end{pmatrix}. \tag{14}$$

In eqn (14), i and j represent the element and respective node numbers, and a_i are obtained by averaging between nodal values. The consistent mass matrix was adopted since numerical trials with this choice produced better results with the particular integration scheme

employed while, at the same time, introducing no significant computational inefficiency due to the coupling of equations.

The integration of the equations of motion (13) is carried out using the following Newmark scheme:

$$\dot{u}_{n+1} = \dot{u}_n + (1-\gamma)\Delta\bar{t}\ddot{u}_n + \gamma\Delta\bar{t}\ddot{u}_{n+1}$$
$$u_{n+1} = u_n + \Delta\bar{t}\dot{u}_n + (\tfrac{1}{2}-\beta)\Delta\bar{t}^2\ddot{u}_n + \beta\Delta\bar{t}^2\ddot{u}_{n+1} \tag{15}$$

where γ and β are the parameters controlling the stability and accuracy of the algorithm and n refers to the increment corresponding to time $\bar{t}$. The explicit central difference scheme is obtained from (15) by setting $\gamma = 0.5$ and $\beta = 0$. Solving $\ddot{u}_{n+1}$ from (15) for non-zero β, defining $\Delta u = u_{n+1} - u_n$ and substituting in (13) gives

$$\mathbf{M}\Delta\mathbf{Q} = (\beta\Delta\bar{t}^2)\mathbf{R}_{n+1} + \Delta\bar{t}\mathbf{M}\dot{\mathbf{Q}}_n + (\tfrac{1}{2}-\beta)\Delta\bar{t}^2\mathbf{M}\ddot{\mathbf{Q}}_n. \tag{16}$$

Note that this integration scheme can be rendered explicit if the nodal force vector R_{n+1} is replaced by R_n. This approximation is not expected to introduce significant error because of the stringent requirement on the time step $\Delta\bar{t}$ necessitated by the stability consideration of this scheme. The error involved is of the same order as that of the central difference method where u_{n+1} is first computed using quantities at n [i.e. $\beta = 0$ in (15b)] and R_{n+1} is evaluated employing this value of u_{n+1}. Equation (16) is particularly suited for our application since the boundary conditions (1) are imposed.

Once the $\Delta\dot{u}$s are determined using (16), $\ddot{u}_{n+1}$ and $\dot{u}_{n+1}$ are obtained from (15b) and (15a), respectively. The incremental quantities are then updated for the next increment. The residual of eqn (13), due to the newly obtained $\mathbf{R}_{n+1}$ (i.e. $\beta\Delta\bar{t}^2\mathbf{R}_{n+1} - \beta\Delta\bar{t}^2\mathbf{M}\ddot{\mathbf{Q}}_{n+1}$) are added to the right-hand side of (13) as a correction for the next increment. The γ and β values employed are specified in the following section.

The updating of the incremental quantities was carried out using an explicit Euler integration method whose stability requirement limits the time step so that the strain increments remain of the order of $m\sigma_Y/E$ (Cormeau, 1975). This implies that the permissible time step diminishes towards zero when the rate-independent limit is approached ($m \to 0$). Other stability criteria limit the time step to the travel time of an elastic wave across the shortest element in the grid. However, these criteria are not operative here and experimenting with the numerical integration of the equations of motion determines the maximum permissible time step (Needleman, 1989).

4. RESULTS AND DISCUSSION

All of the numerical results produced for rate-dependent behaviour correspond to a material whose uniaxial response is described by eqn (8) with $\varepsilon_Y = \sigma_Y/E = 0.001$, $N = 0.15$, $m(E/\sigma_Y)^N = 0.02$ and $\dot{\varepsilon}_R = 0.000137$. The calculations for the rate-independent solid were carried out for an elastic–plastic solid for which (8b) was replaced by the conventional form $(\sigma/\sigma_Y) = (E\varepsilon/\sigma_Y)^N$ with the same σ_Y/E and N values as given above.

In the computations, a solid cylinder with $R_0/L_0 = 4$ was considered. A geometric imperfection of the type (10) was introduced with $\kappa = 4$ and a ξ value which corresponds to an initial area defect of $(\Delta A/A_0) = 0.0025$ at the mid-section $x = 0$. The undeformed geometry is depicted in Fig. 2 and the effect of this long-wavelength type of imperfection on neck growth was examined. A grid consisting of 100 unidimensional equidistant bar elements was employed. The boundary condition (1) was imposed in a non-dimensional form as $\Delta U/L_0$ $(= \dot{U}\Delta\bar{t})$ at $x = L_0$.

We first compare the results for a rate-independent solid with a pull speed $(\dot{U}/c) = 0.5 \times 10^{-5}$ to that of the rate-dependent solid with $(\dot{U}/c) = 0.125 \times 10^{-3}$. The constant β of equation (15) was taken as 1/6 for both cases. The rate-independent solid was analysed using $\gamma = 0.5$. For the rate-dependent solid some artificial damping was introduced in the elastic region with $\gamma = 0.6$ for $\varepsilon \leqslant \varepsilon_Y$ while $\gamma = 0.5$ was employed for $\varepsilon \geqslant \varepsilon_Y$. In view

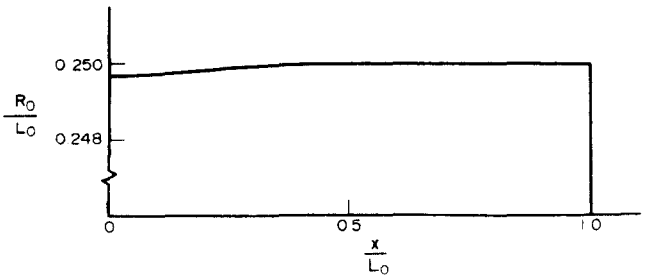

Fig. 2. Specimen geometry used in the numerical analysis with a long-wavelength type of imperfection.

of the extremely low pull speed considered for the rate-independent solid, this response can be regarded as quasi-static. Results are shown in Fig. 3 where the loads carried at the neck ($x = 0$) and the end ($x = L_0$) sections are plotted against the end displacement U/L_0 in the elastic range and initial plastic region for both cases. With the low pull speed considered for the rate-independent material, the loads at $x = 0$ and $x = L_0$ become almost identical, once a very small amount of elongation $[(U/L_0) \geqslant 0.000015]$ is attained. For the rate-dependent solid, with $(\dot{U}/c) = 0.125 \times 10^{-3}$, a step-like rise pattern is observed for the loads at the neck ($x = 0$) and the end ($x = L_0$) sections for all of the elastic region. This is expected, with the lag in the two loads corresponding to the time required for a wave to travel the length of the specimen. There is a slight difference from the analytical solution which predicts an exact step function rise corresponding to elastic waves with $\Delta\varepsilon = \dot{U}/c$. This is inevitable in a numerical method such as this with $\gamma = 0.6$. Once the plastic strains set in the fluctuations in loads slowly attenuate, and these fluctuations eventually become indistinguishable for the rate-dependent case after an elongation of $(U/L_0) \geqslant 0.002$.

The load elongation curves for the above mentioned cases in the plastic region are shown in Fig. 4. As mentioned above, the results for the rate-independent solid can be taken to be quasi-static due to the low pull speed employed $[(\dot{U}/c) = 0.5 \times 10^{-5}]$. From Fig. 4 we note that necking for the rate-independent solid occurs at an elongation level of $(U/L_0) \cong 0.138$ and when the maximum strain at the end section reaches $\varepsilon = 0.124$. This critical value of necking strain ε^{cr} at the uniform section ($x = L_0$) for a relative imperfection of $(\Delta A/A_0) = 0.0025$ can also be recovered from the relation given by Hutchinson and

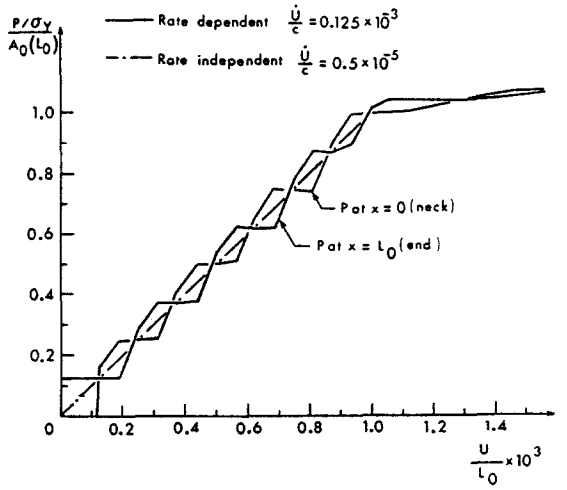

Fig. 3. Load–elongation curves in the elastic range for rate-dependent and rate-independent solids.

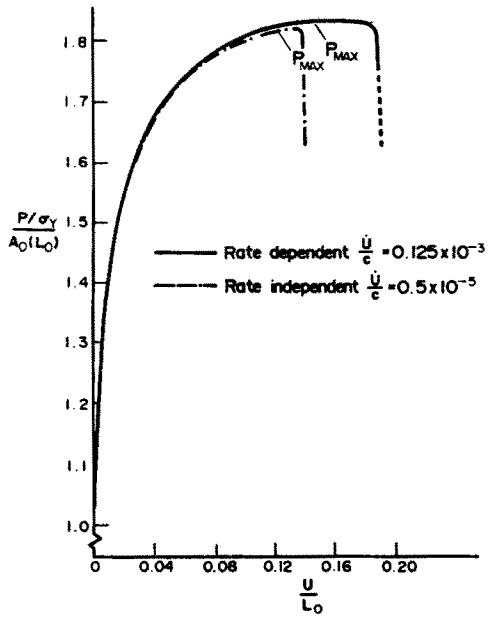

Fig. 4. Load–elongation curves for rate-dependent and rate-independent solids.

Neale (1977) for rate-independent material behaviour:

$$\frac{\varepsilon^{cr}}{N}\exp\left(1-\frac{\varepsilon^{cr}}{N}\right)=\left(1-\frac{\Delta A}{A_0}\right)^{1/N}. \tag{17}$$

When inertia is included, each value of imperfection and pull speed has a distinct effect on the onset of necking. This aspect is not reflected in the analysis of Regazzoni *et al.* (1986), where the assumption of a uniform strain state $\varepsilon = N$ is used as the initial condition for the dynamic problem. Such an approximation can only be considered realistic in the limit $(\Delta A/A_0) = 0$.

The quasi-static analysis for the rate-dependent solid with $(\dot{U}/c) = 0.125 \times 10^{-3}$ becomes almost the same as the dynamic solution of Fig. 4 after the elongation (U/L_0) exceeds $2\varepsilon_Y$. Due to the relatively low pull speed employed here, the retardation effect of inertia arises only at the very late stages of the loading history, as shown with the enlarged scale of Fig. 5. The differences between the two solutions represented in Fig. 4 are thus

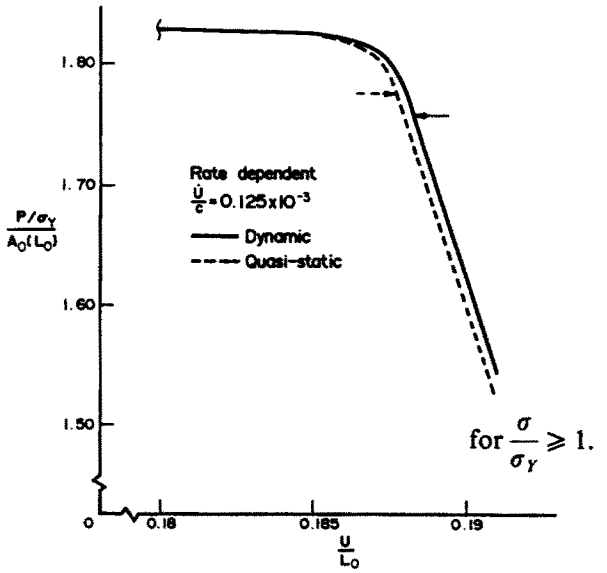

Fig. 5. Comparison of the dynamic and quasi-static responses for rate-dependent solid.

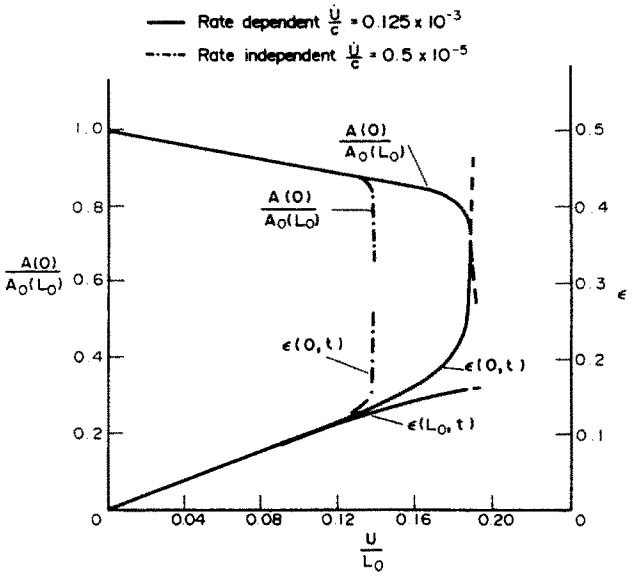

Fig. 6. Development of normalized area at the mid-section ($x = 0$) and strain as a function of elongation U/L_0 for rate-dependent and rate-independent solids.

essentially the result of material strain-rate sensitivity (Hutchinson and Neale, 1977; Needleman and Tvergaard, 1985). The dashed portion of the curve for the rate-dependent solid (Fig. 4) corresponds to the part of the loading history during which the deformations are localized in the element located at the neck ($x = 0$) while the rest of the bar is undergoing elastic unloading. Thus, the length of the necked region in this dashed part of the loading history is always determined by the length of the element bordering $x = 0$. This mesh-sensitivity aspect of the one-dimensional analysis will be discussed later.

The differences between the dynamic and quasi-static responses for the rate-dependent solid are depicted in Fig. 5. While there is essentially no difference in the response for the early stages of the load-deformation history [with the exception of the initial response for $(U/L_0) < 2\varepsilon_Y$], the retardation effect due to inertia, small as it may be here, can be observed for $(U/L_0) > 0.180$. The basic mechanism of the deformation pattern for the dynamic solution is the same as for the quasi-static case. An elastic unloading wave starts at the uniform section ($x = L_0$) at $(U/L_0) \cong 0.185$ for both cases and travels towards the neck. The horizontal arrows in Fig. 5 indicate the arrival point of this wave at the neck element, after which the solution becomes mesh sensitive. Clearly, the presence of inertia retards the propagation of the elastic unloading wave, although it has no prior distinguishable effect for the slow pull speed considered.

The evolution of the neck as well as the strain at $x = 0$ are depected in Fig. 6 for the two solutions represented in Fig. 4. Also shown in the same figure is the strain history of the end section ($x = L_0$) for the rate-dependent solid. Here too, the dashed portion of the curves for the rate-dependent solid corresponds to the mesh-sensitive part of the solution.

The evolution of the specimen geometry is displayed in Fig. 7 where the bar profiles for the rate-dependent solid at elongations $(U/L_0) = 0.159$ and 0.1884 are shown. The profile $(U/L_0) = 0.159$ corresponds to the elongation where the load reaches a maximum. At this stage the deformation of the specimen is essentially uniform, as also evident from the results of Fig. 6. The second geometry depicted in Fig. 7 corresponds to the stage soon after which the deformation localizes in the element at the neck, while the rest of the specimen is unloading elastically. At $(U/L_0) = 0.1884$ considerable localization has taken place with a normalized neck area of $(A(0)/A_0(L_0)) = 0.707$ and $\varepsilon(0, t) = 0.3444$, as opposed to the respective values of 0.853 and 0.1586 at the end section. The stresses along the x-axis for the two geometries are also depicted in Fig. 7. When the strong gradient in the stress distribution develops at the neck at $(U/L_0) = 0.1884$ the strain rate at the same location reaches $(\dot{\varepsilon}^P/\dot{\varepsilon}_R) = 73.12$, while the neighbouring element is deforming with $(\dot{\varepsilon}^P/\dot{\varepsilon}_R) = 0.113$

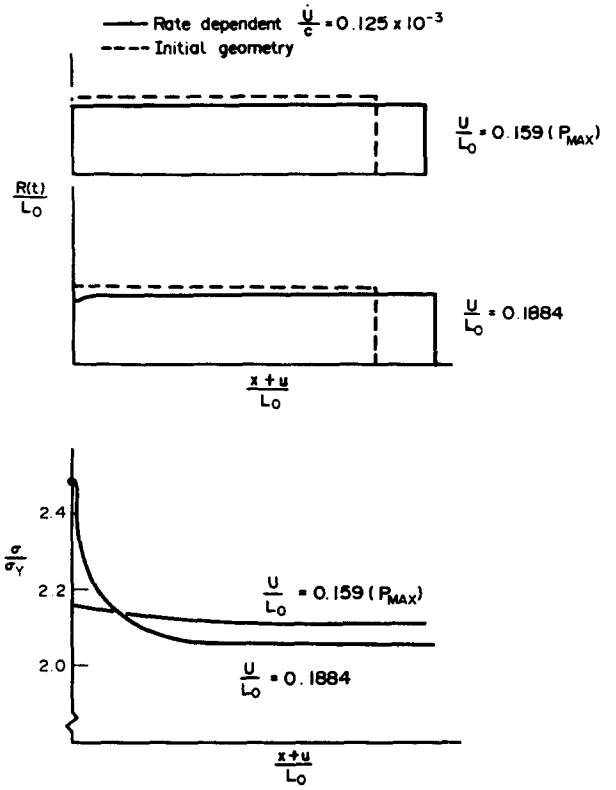

Fig. 7. Specimen profiles for rate-dependent solid and the corresponding stress distributions at elongation levels indicated.

and the rest of the specimen is unloading elastically. For the pull speed ($\dot{U}/c = 0.125 \times 10^{-3}$) considered, it can therefore be concluded that the stresses at the neck are bounded by the solid curve corresponding to $\dot{\varepsilon}^P = 100\dot{\varepsilon}_R$ in Fig. 1. From Fig. 7 we also observe that the stresses (and strains) reach their maximum value at the neck and decrease thereafter continuously to a minimum value at the end with a very steep gradient around the neck for the necked geometry [i.e. for $(U/L_0) = 0.1884$]. In Regazzoni *et al.* (1986) the reversal in the stress and strain gradients occurs at the interface between their geometric defect and the uniform section of the specimen. In their simulation elastic unloading occurs at this interface. This is a result of the initial condition employed in their analysis, where a uniform state of strain $\varepsilon = N$ is assumed along the entire bar before geometric effects are introduced and the dynamic problem is analyzed.

The initial undeformed specimen geometry employed here (Fig. 2) has an imperfection of type (10) and corresponds to an area defect of $(\Delta A_0/A_0(L_0)) = 0.0025$. This long-wavelength type defect extends to more than 1/4 of the length of the specimen and is similar in shape to the imperfection prescribed by Regazzoni *et al.* (1986). The evolution of the neck into one single neck element, as discussed previously, is associated with the sharp strain gradients resulting from the one-dimensionalization of the formulation. This suggests that it is the relative depth, but not the length of the imperfection, that has an effect on the strain localization. As discussed by Hutchinson and Neale (1977), with regard to quasi-static behaviour, we expect that a three-dimensional analysis will produce a smoother neck transition combined with smoother strain gradients. Another limitation of the one-dimensional analysis is that at high levels of pull speed, radial inertia effects may no longer be negligible (Regazzoni *et al.*, 1986).

The localization of strains into one single element at the neck renders the one-dimensional finite element analysis highly mesh-dependent. To study the effect of mesh size on the computed response, we compare the quasi-static rate-dependent solution for $(\dot{U}/c) = 0.125 \times 10^{-3}$, for two different meshes. These quasi-static rate-dependent analyses

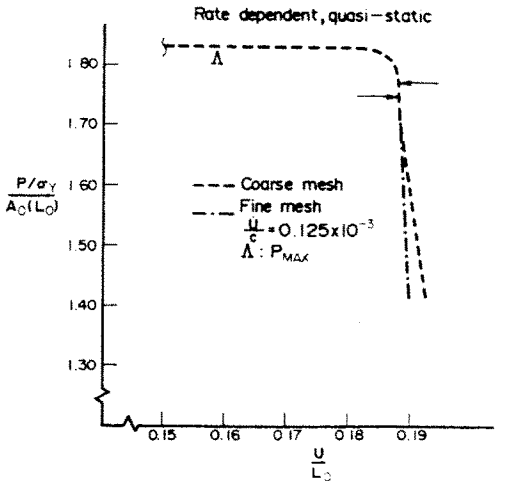

Fig. 8. Mesh sensitivity of the load–elongation response for rate-dependent quasi-static behaviour.

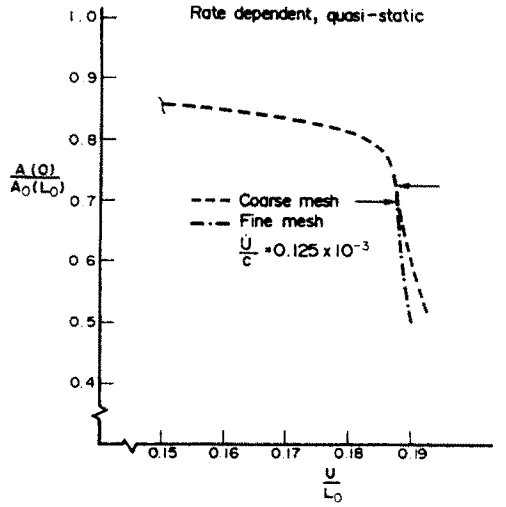

Fig. 9. Mesh sensitivity of the evolution of the normalized area with elongation.

were carried out employing a one-dimensional finite element program based on (7) and the viscoplastic uniaxial law (8). One solution used in this comparison is that of the previous quasi-static rate-dependent study with the mesh size prescribed earlier. A finer mesh was produced by dividing the element bordering $x = 0$ into two equidistant elements. Indistinguishable results are obtained for both meshes until localization takes place. The results for $(U/L_0) > 0.15$ are displayed in Figs 8 and 9. These correspond to the plots of the load and the neck area versus the elongation, respectively. In these figures, the horizontal arrows indicate the points after which localization is concentrated into one single element at the neck. These occur at approximately the same elongation level for both solutions. With additional elongation, however, the differences between the two meshes grow very rapidly, the fine mesh resulting in a much steeper response. Once the elastic unloading wave reaches the neck element, all of the end displacement imposed, plus that arising from the elastic unloading of all the rest of the mesh, is absorbed by the neck element. This implies that the stretch and the strain become infinite when the element size l goes to zero. Therefore, after the arrival of the elastic unloading wave at the neck, the solution consists of a sharp drop to zero of the variables plotted in Figs 8 and 9. Since the numerical solution cannot produce this result with a finite length neck element, the parts of the curves following the horizontal arrows diminish in accuracy.

5. CONCLUSION

A one-dimensional finite element program has been developed to study necking instability in a round specimen under tension. Viscoplastic material behaviour as well as effects of inertia are incorporated in the large-strain Lagrangian formulation employed.

Based on computations simulating the whole load-deformation-time response, our results indicate that the overall features of dynamic necking are the same as for the quasi-static case when necking is analysed using an imperfection-growth approach. Further, it is shown that if a homogeneous strain state prior to the introduction of a geometric imperfection is assumed, as in Regazzoni *et al.* (1986) and Taylor *et al.* (1978), a good estimate of the elongations corresponding to this uniform state is required to obtain accurate results. Also, predictions based on quasi-static analyses will furnish conservative estimates since the inclusion of inertia has a further stabilizing effect, as observed in this and the above studies.

The one-dimensional analysis performed is shown to be mesh-sensitive once the imperfection growth leads to rapid strain localization. The length of the necked region under continued plastic deformation is determined by the length of the single element at the neck while the rest of the specimen is unloading elastically. It is important to note that this mesh sensitivity is existent for both the rate-dependent and rate-independent solids due to the one-dimensional approach adopted. It is not the same as the pathological mesh sensitivity discussed by Needleman (1988) for shear band formation in rate-independent solids.

Acknowledgements—This work was supported by the Natural Sciences and Engineering Research Council of Canada and the Government of the Province of Québec (Programme FCAR).

REFERENCES

Clifton, R. J. (1972). Plastic waves: theory and experiment. In *Mechanics Today* (Edited by S. Nemat-Nasser), Vol. 1, p. 102. Pergamon, Oxford.

Cormeau, I. C. (1975). Numerical stability in quasi-static elasto-viscoplasticity. *Int. J. Numer. Meth. Engng* **9**, 109–127.

Hutchinson, J. W. and Neale, K. W. (1977). Influence of strain-rate sensitivity on necking under uniaxial tension. *Acta Met.* **25**, 839–846.

Lahoud, A. E., Tuğcu, P. and Neale, K. W. (1986). Finite element schemes for large-strain plasticity computations. In *Computer Modelling of Fabrication Processes and Constitutive Behaviour of Metals* (Edited by J. J. M. Too). CANMET, Ottawa.

Needleman, A. (1988). Material rate dependence and mesh sensitivity in localization problems. *Computer Meth. Appl. Mech. Engng* **67**, 69–85.

Needleman, A. (1989). Dynamic shear band development in plane strain. *ASME J. Appl. Mech.* **56**, 1–9.

Needleman, A. and Tvergaard, V. (1985). Material strain-rate sensitivity in round tensile bars. In *Plastic Instability* (Edited by J. Salençon). Presses des Ponts et Chaussées, Paris.

Regazzoni, G., Johnson, J. N. and Follansbee, P. S. (1986). Theoretical study of the dynamic tensile test. *ASME J. Appl. Mech.* **53**, 519–528.

Taylor, J. W., Harlow, F. H. and Amsden, A. A. (1978). Dynamic plastic instabilities in stretching plates and shells. *ASME J. Appl. Mech.* **45**, 105–110.